

Understanding the Long-term Trend of Organic Aerosol and the Influences from Anthropogenic Emission and Regional Climate Change in China

Wenxin Zhang¹, Yaman Liu^{1,2}, Man Yue^{1,2}, Xinyi Dong^{1,3,4}, Kan Huang^{5,6,7}, Minghuai Wang^{1,4}

5 ¹School of Atmospheric Science, Nanjing University, Nanjing, 210023, China

²Zhejiang Institute of Meteorological Sciences, Hangzhou, 310008, China

³Frontiers Science Center for Critical Earth Material Cycling, Nanjing University

⁴Joint International Research Laboratory of Atmospheric and Earth System Sciences & Institute for Climate and Global Change Research, Nanjing University, Nanjing, 210023, China

10 ⁵Department of Environmental Science and Engineering, Shanghai Key Laboratory of Atmospheric Particle Pollution and Prevention (LAP3)

⁶Institute of Eco-Chongming, Shanghai, China

⁷IRDR ICoEon Risk Interconnectivity and Governance on Weather/Climate Extremes Impact and Public Health, Fudan University, Shanghai, China

15 *Correspondence to:* Xinyi Dong (dongxy@nju.edu.cn)

Abstract. Organic aerosol (OA) is a major type of fine particulate matter. OA shows a large variability influenced by anthropogenic emissions, vegetation, and meteorological changes. Understanding OA trends is crucial for air quality and climate studies, yet changes in OA over time in China are poorly documented. This study applied the Community Atmosphere Model version 6 with comprehensive tropospheric and stratospheric chemistry (CAM6-Chem) to investigate long-term OA

20 trends in China from 1990 to 2019 and identify the driving factors. The simulations agreed well with ground-based measurements of OA from 151 observational sites and the CAQRA reanalysis dataset. Although OA trends showed a modest

5.6% increase, this resulted from a significant -8.1% decrease in primary organic aerosols (POA) and a substantial 32.3% increase in secondary organic aerosols (SOA). Anthropogenic emissions of POA and volatile organic compounds (VOC) were the dominant contributors to these trends. While biogenic VOC (BVOC) played a secondary role in SOA formation, significant

25 changes were observed in specific sub-species: isoprene-derived SOA decreased by -18.8% due to anthropogenic sulfate reduction, while monoterpene-derived SOA increased by 12.3% driven by enhanced emissions from rising temperatures. Our

study found through sensitivity experiments a negligible response of monoterpene-derived SOA to changes in anthropogenic nitrogen oxides (NO_x) emissions as a net effect of changes in multiple pathways. This study highlights the complex interplay between POA reduction and SOA growth, revealing notable OA trends in China and the varying roles of both anthropogenic

30 and biogenic emissions.

1. Introduction

PM_{2.5} (particulate matter less than or equal to 2.5 micrometers in diameter) is a standard air pollutant and attracts numerous research attention during the past decade. Ground level mass concentration of PM_{2.5} was found to gradually increase during 2000-2013 and then decreased since 2014 in China (An et al., 2019; Lin et al., 2018; Ma et al., 2016). The trend of PM_{2.5} is believed to be driven primarily by China's emission control policies (Lu et al., 2020; Tong et al., 2020) and regional climate change over East Asia, which affects the dispersion condition (Xu et al., 2022). Organic aerosol (OA) is an important component of PM_{2.5} as it can contribute up to 77% of total fine mode particles during haze pollution episode (An et al., 2019; Zhong et al., 2021). Despite its significance, there have been limited studies involving long-term continuous observations of OA. Unlike PM_{2.5}, the observational gaps restrict our understanding of historical trends in OA, making it challenging to access air quality changes accurately and formulate effective environmental policies. While a few existing modeling studies have explored recent changes in OA in China, they often cover only limited time periods or specific years (Chen et al., 2024a; Zheng et al., 2023b).

OA consists of primary organic aerosols (POA) and secondary organic aerosols (SOA). POA is largely emitted from anthropogenic sources such as vehicle emissions, residential biofuel usage, and industrial activities, as well as biomass burning. Consequently, POA emissions are usually intensive (Fadel et al., 2021; Kanellopoulos et al., 2021) in urban areas (Liu et al., 2023) with their impact being primarily localized due to dependence on anthropogenic sources. Control of POA emissions has been effective in reducing PM_{2.5} concentrations, as observed in regions like the Western United States (Pye et al., 2019). In China, studies have also reported a significant contribution of POA to PM_{2.5}. Huang et al. (2019) discovered that POA emerges as the primary constituent during pollution episodes in the North China Plain region (Huang et al., 2019). Zheng et al. (2023a) found a decrease of 11.8 $\mu\text{g m}^{-3}$ in OA concentrations at Beijing over 2005-2018, with most of the decrease coming from POA (Zheng et al., 2023a).

On the other hand, SOA is mainly produced through complex transformations of volatile organic compounds (VOC) emitted from both anthropogenic and biogenic sources (Hallquist et al., 2009; Qin et al., 2018; Srivastava et al., 2017; Zhang et al., 2007). These VOC undergo multiple oxidation processes in the atmosphere, making SOA formation sensitive to chemical reactions, as well as meteorological conditions (An et al., 2019; Fan et al., 2020; Hu et al., 2017). In Southern China, biogenic VOC (BVOC), primarily monoterpenes and isoprene, are significant contributors to SOA formation, particularly during summer due to warm temperatures and extensive vegetation (Guenther et al., 2012). Given that SOA formation is affected by both anthropogenic and natural factors, the response of OA to changing emission and climate conditions is likely nonlinear.

In the context of global warming, China has made considerable efforts to reduce anthropogenic emissions through a range of climate policies (Cai et al., 2017; Cui et al., 2020; Feng et al., 2019; Zheng et al., 2018). These measures have led to reductions

in both POA and SOA concentrations. However, biogenic SOA (BSOA) also plays an important role in determining OA trends
65 as it may change due to anthropogenic emission change. For example, studies indicate that BSOA produced from isoprene-
epoxydiols (IEPOX) has significantly decreased in the Southeast United States due to reductions in anthropogenic SO_2
emissions (Hoyle et al., 2011; Liu et al., 2021b; Qin et al., 2018; Shilling et al., 2013; Shrivastava et al., 2019), and a similar
response was also reported in China (Dong et al., 2022). Likewise, monoterpene-derived SOA (SOA_{MT}) is sensitive to nitrogen
oxides (NO_x) concentrations, and interactions between NO_x and BVOC can alter the oxidation pathways and ultimately affect
70 BSOA formation (Jo et al., 2019; Xu et al., 2021; Zhang et al., 2018).

The abovementioned studies suggest that the long-term trends in OA might be a net result of the opposing trends in its sub-species, driven by multiple anthropogenic and natural factors. Nevertheless, existing modeling studies largely attribute OA trends to emission changes without detailed consideration of different sub-species. Moreover, the interactions between BVOC
75 and changing climate conditions complicate predictions of BSOA responses, hindering accurate forecasts of future OA trends. Diagnostically investigating OA trends and driving factors is therefore crucial to ensure a more comprehensive assessment of air quality changes. Given the limited availability of long-term observational data, this study employs a modeling tool along with available observation and reanalysis dataset to explore the long-term trends of OA in China from 1990 to 2019, considering contributions from different sub-species. This analysis aims to support future air pollution control strategies by
80 providing a better understanding of OA and its driving factors, thereby enabling more effective management of air quality in the face of ongoing climate change.

2. Data and Methods

2.1 Model Configuration

This study uses the Community Atmospheric Model version 6 with comprehensive tropospheric and stratospheric chemistry
85 (CAM6-Chem) from the Community Earth System Model version 2.1.0 (CESM2.1.0). The gas-phase chemistry is represented by the Model for Ozone and Related chemical Tracers (MOZART) chemical mechanism (MOZART-TS2) including comprehensive isoprene and monoterpenes chemistry (Schwantes et al., 2020). The aerosol model utilizes the four-mode version of the Modal Aerosol Module (MAM4) (Liu et al., 2016) and employs the Volatility Basis Set (VBS) approach (Donahue et al., 2006; Hodzic et al., 2016) to simulate SOA formation. VOC (isoprene, glyoxal, monoterpenes, sesquiterpene,
90 benzene, toluene, lumped xylenes, intermediate volatile organic compounds and semi-volatile organic compounds) are oxidized to produce five different types of volatile SOA gaseous precursors, with volatilities corresponding to effective saturation concentrations (C^*) of 0.01, 0.1, 1.0, 10.0, and 100.0 $\mu\text{g}/\text{m}^3$ at 300 K, respectively (Tilmes et al., 2019). Heterogeneous production of isoprene-epoxydiol-derived SOA (SOA_{IE}) is represented within the coupled Model for Simulating Aerosol Interactions and Chemistry (MOSAIC) (Jo et al., 2019, 2021; Zaveri et al., 2008, 2021) mechanism. The

95 photolysis rate of monoterpene-derived SOA is updated based on our previous work (Liu et al., 2023). Aerosol wet removal
scheme uses the Cloud Layers Unified By Binormals (CLUBB) scheme to unify shallow convective and stratiform clouds,
coupled with the two-moment cloud microphysics scheme by Gettelman and Morrison (2015) (MG2) for aerosol activation
and removal (Gettelman and Morrison, 2015). For deep convective clouds, the scheme employs the parameterization by Zhang
and McFarlane (1995) (ZM95) and relies on empirical parameters for estimating aerosol wet removal processes (Zhang and
100 McFarlane, 1995).

We conducted long-term simulations covering the period from 1990 to 2019. The horizontal resolution of the simulations is
set to 0.95° for latitude and 1.25° for longitude, with 32 vertical layers extending to approximately 40 kilometers. The
simulation has a spin-up time of 1 year and a relaxation time of 50 hours to investigate surface OA trends. Natural emissions
105 are calculated online using the Model of Emissions of Gases and Aerosol from Nature version 2.1 (MEGAN2.1), which is
coupled to the CESM model (Emmons et al., 2020; Guenther et al., 2012). Anthropogenic emissions from 1990 to 2019 were
sourced from the multi-resolution emission inventory for China (MEIC, <http://www.meicmodel.org>) (Li et al., 2017).
Intermediate volatile organic compounds (IVOC) and Semi-volatile organic compounds (SVOC) emissions were scaled
based on POA emissions and non-methane VOC emissions (Chang et al., 2022; Tilmes et al., 2019), with specific formulas
110 provided in the supplement. We used the Modern-Era Retrospective analysis for Research and Applications (MERRA2)
reanalysis data (Gelaro et al., 2017) for meteorological constraints.

To distinguish the effects of biogenic emissions and anthropogenic NOx emissions on SOA_{MT} , we conducted additional
sensitivity simulations by applying scaling factors for monoterpene and NOx emissions respectively. Monoterpene emissions
115 are higher in summer (Zhang et al., 2018), and 2013 saw the peak monoterpene emissions (Fig. 8(a)), while NOx
concentrations reached a secondary peak (Fig. 8(b)). Therefore, we have selected July 2013 for sensitivity simulations to better
capture SOA_{MT} 's response to both emission types. A benchmark simulation was conducted and denoted as 100nudging, which
has the same configuration as the long-term simulation but with a 0.5-hour relaxation time to minimize the impact of
120 meteorological fields (Liu et al., 2021a; Tilmes et al., 2019). One type of sensitivity experiment was monoterpene emission
experiments, and the two sets of experiments were named 0.5MTERP and 2MTERP. Their model configurations were the
same as those of 100nudging, but the monoterpene emissions were respectively set to 0.5 and 2 times the 100nudging
emissions. Their differences relative to 100nudging indicated the impact of monoterpene emissions disturbance on SOA_{MT}
formation. The other type of sensitivity experiment was NOx emission experiments, and the two sets of experiments were
125 named 0.5NOx and 2NOx. Their model configurations were also the same as those of 100nudging, but the NOx emissions
were respectively set to 0.5 and 2 times the 100nudging emissions. Their differences relative to 100nudging indicated the
impact of NOx emissions disturbance on SOA_{MT} formation.

The model used in this study classifies monoterpenes into four categories: α -pinene, β -pinene, limonene, and myrcene. In the following sections, these will be collectively referred to as monoterpenes. In this study we constrained BSOA as the summary 130 of SOA_{MT} and SOA_{IE} to focus on these two most important contributors. It shall be mentioned that isoprene and monoterpenes make the most contributions to BVOC in China (Ding et al., 2016). For this reason, BVOC emissions in this study are constrained to the sum of isoprene and monoterpenes emissions, allowing for a more focused analysis of the primary contributors. This study specifically focuses on the impact of aerosols derived from these compounds on OA trends.

2.2 Observations

135 We used observations from a number of different sources to evaluate the simulation performance of major aerosol species as well as key intermediates. We used ground-based measurements compiled by Miao et al. (2021) and Chen et al. (2024), which provided mean mass concentrations of surface OA, POA, and SOA in China from 2013 to 2019, along with the corresponding station locations (Chen et al., 2024a; Miao et al., 2021). A total of 151 measurements were included by removing duplicate values. We also used the high-resolution simulation dataset of PM_{2.5} composition over China (CAQRA-aerosols) provided by 140 the National Natural Science Foundation Air Pollution Complex Major Research Plan Data Integration Project (Project Number: 92044303, <https://www.capdatabase.cn>). The CAQRA-aerosols data were developed using emission inversion and high-resolution numerical simulation techniques (Kong et al., 2021). The CAQRA-aerosols data provided mass concentrations 145 of organic carbon (OC) rather than OA (Kong et al., 2021). The root mean square error of OC on the monthly average concentration scale was 12.0 $\mu\text{g}/\text{m}^3$, with a mean bias of 0.03 $\mu\text{g}/\text{m}^3$ (0.17%) (Kong et al., 2021). We used OA/OC ratios (1.19- 3.04) to convert OC to OA concentrations (Malm and Hand, 2007) to facilitate comparison with simulation results. Since ratios vary with site and season, we used the mean value of 1.8 recommended by Malm and Hand (2007) as the conversion factor (Malm and Hand, 2007). To understand the model performance for simulating air pollutants, we also analyzed them by comparing them with the output values at the corresponding times and locations in the model. The 24h average PM_{2.5} and ozone (O₃) data from the China Environmental Monitoring Terminal (CEMT) National Urban Air Quality Real-Time 150 Distribution Platform (NUAQRDP) (<https://air.cnemc.cn:18007/>) were used to analyze changes in surface aerosol concentrations over the period 2014-2019.

Moreover, we used MODIS Level3 Collection 6.1 monthly aerosol optical depth (AOD) data as an indicator for column density of fine size aerosols. The 550 nm AOD data were retrieved using the combined Dark Target-Deep Blue algorithm (Levy et al., 155 2013), with monthly averaged data covering the years 2000-2019 at a spatial resolution of 1°. Performance of NO_x simulation was also assessed using nitrogen dioxide (NO₂) column concentrations monitored by the OMI (Ozone Monitoring Instrument) Level-3 on board NASA's AURA satellite (<https://disc.gsfc.nasa.gov/datasets?keywords=OMI&page=1>), with daily averaged data covering the period 2000-2019 at a spatial resolution of 0.25°.

3. Results and Discussions

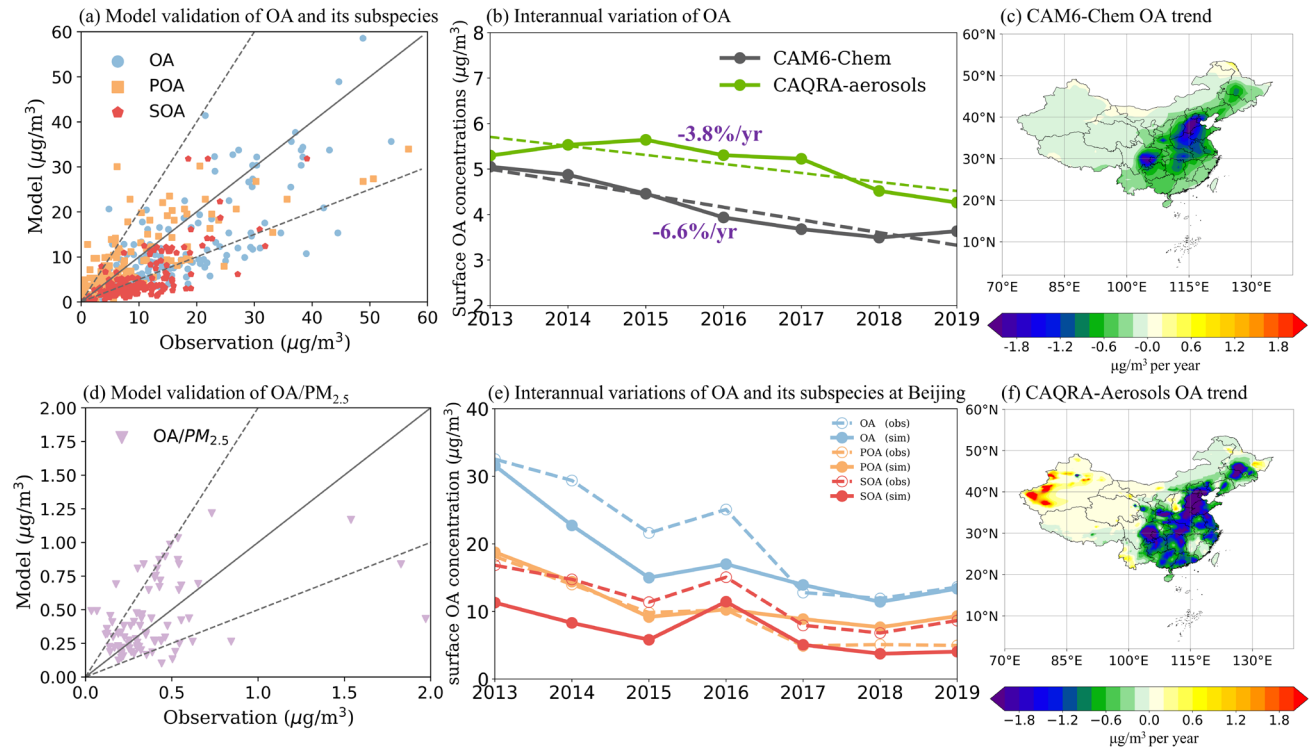
160 3.1 Evaluation of Model Performance

Performance of the model was evaluated by comparing simulation results with ground-based observations, the CAQRA-aerosols dataset and satellite products mentioned in Section 2. The results of the baseline simulation were compared with observations from multiple sources. Overall, the model can generally reproduce the spatial distributions and mass concentrations of OA and its components (Fig.S1). By validation with observations from Miao et al. (2021) and Chen et al. 165 (2024), the modelled normalized mean bias (NMB) of surface OA, POA, and SOA were -34.5%, -7.4%, and -64.8%, respectively. Although there was a general underestimation of surface OA by the model, the simulations showed close agreement with measurements, with a coefficient of determination (R^2) by 0.8. The capability of CAM-Chem in simulating OA over China was generally well consistent with other modeling studies. For example, Qin et al. (2018) utilized the 170 Community Multiscale Air Quality (CMAQ) model (v5.0.2) to evaluate BSOA and reported an NMB of -70% (Qin et al., 2018); Zheng et al. (2023b) employed the Weather Research and Forecasting model (WRF, v3.9)–CMAQ/2D-VBS modeling system and observed an NMB of -20% for POA (Zheng et al., 2023b).

Our model simulated spatial distribution of OA was in good agreement with the CAQRA-aerosols dataset. Both our model and the dataset indicated relatively higher OA concentrations in Eastern China and lower concentrations in Western China 175 (Fig.S2). The CAQRA-aerosols dataset showed that OA has strong seasonality in China, with the highest average mass concentrations in winter and the lowest in summer. Our model simulations reproduced this seasonal characteristic well (Fig.S3). The results of both the model and the CAQRA-aerosols dataset indicated a decreasing trend in OA concentrations in China (Fig.1(b)). Notably, there was good spatial consistency, with a significant decrease observed in Eastern China, particularly in the North China Plain region (Fig.1(c,f)). This decreasing trend was especially pronounced in Beijing. Given that only the 180 Beijing site had continuous ground-based observations over multiple years from Miao et al. (2021) and Chen et al. (2024), we further evaluated the long-term simulation results for this site. The simulation values showed good agreement with the observed values, reflecting a consistent trend over the years (Fig.1(e)).

In terms of $PM_{2.5}$ simulation, the model slightly underestimated observation by -19.2% (Fig.S6(a)). This might be at least 185 partially because of coarse model grid resolution while CEMT observational sites are mostly within urban area. We then compared the simulation with observation for the contribution of OA to $PM_{2.5}$, showing good performance with an NMB of 5.6%. Observed OA/ $PM_{2.5}$ ratio was calculated by paring OA measurements reported in Miao et al. (2021) and Chen et al. (2024) with CEMT $PM_{2.5}$ observations during the same period, which fall into the same CAM6-Chem model grid. Due to lack of synergic collected observations of aerosol subspecies, we didn't validate the contributions from other subspecies but focus 190 on OA only. The moderate underestimations of OA and $PM_{2.5}$ but relatively better performance for simulating OA/ $PM_{2.5}$ ratio suggested that although the model may have deficiencies to reproduce the absolute concentrations of OA, it was able to capture

the contribution from OA correctly. It also implied that there might be systematic bias within the modeling system affecting underestimations of aerosol mass concentrations such as coarse grid resolution. Our recent study thoroughly evaluated CAM-Chem simulation of PM_{2.5} in China and reported that a finer grid (~0.25°) would substantially lower modeling bias, especially over complex terrains during haze episodes (Yue et al., 2023). The fine grid version was not employed in this study as it's not compatible with MOSAIC module yet, and we consider the heterogeneous chemistry of SOA and thermodynamic equilibrium of nitrate represented by MOSAIC is more important for this study to focus on long-term trend of OA and subspecies.

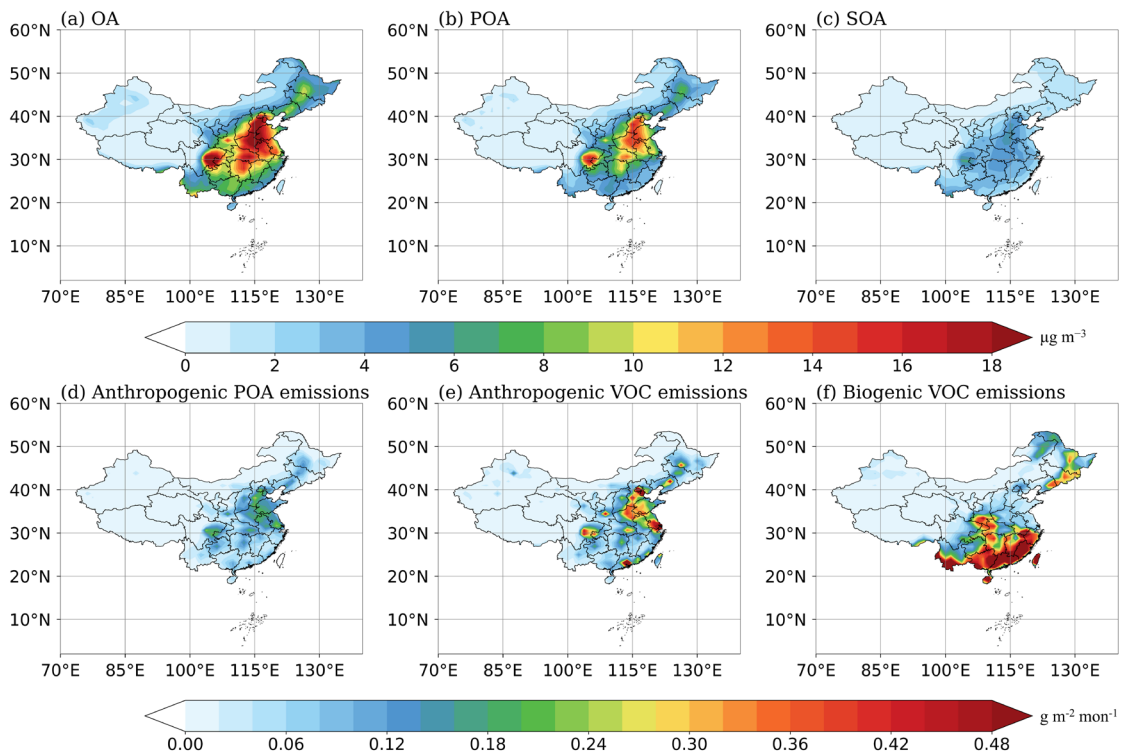


200 **Figure 1: (a) Validation of modelled organic aerosols (OA), primary organic aerosols (POA), and secondary organic aerosols (SOA)** based on ground-based measurements compiled by Miao et al. (2021) and Chen et al. (2024) (unit: $\mu\text{g m}^{-3}$). (b) 2013 to 2019 205 interannual variation of average surface organic aerosol (OA) concentrations in CAM6-Chem (dark grey) and the CAQRA-aerosols dataset (green) (unit: $\mu\text{g m}^{-3}$). The trend lines (dotted line) are based on linear regression fitting. (c) 2013 to 2019 CAM6-Chem modelled annual long-term trend of surface OA concentrations (unit: $\mu\text{g m}^{-3}$ per year). The trend is calculated by linear regression on an annual scale over 1990-2019. (d) Validation of modelled OA/PM_{2.5} based on OA measurements compiled by Miao et al. (2021) and Chen et al. (2024) and PM_{2.5} observations from the National Urban Air Quality Real-time Release Platform of China Environmental Monitoring Station. (e) Interannual variation of average surface OA, POA and SOA concentrations ($\mu\text{g m}^{-3}$) at Beijing site from 2013 to 2019 in CAM6-Chem (solid line; sim) and ground-based measurements compiled by Miao et al. (2021) and Chen et al. (2024) (dashed line; obs). (f) 2013 to 2019 annual long-term trend of surface OA concentrations (unit: $\mu\text{g m}^{-3}$ per year) 210 in the CAQRA-aerosols dataset. The trend is calculated by linear regression on an annual scale over 1990-2019.

3.2 Trend and attribution of Surface OA

In this section we first briefly introduced the general characteristics (e.g., concentrations, main sub-species, spatial distribution) of simulated OA, and then investigated the overall change of OA through the study period.

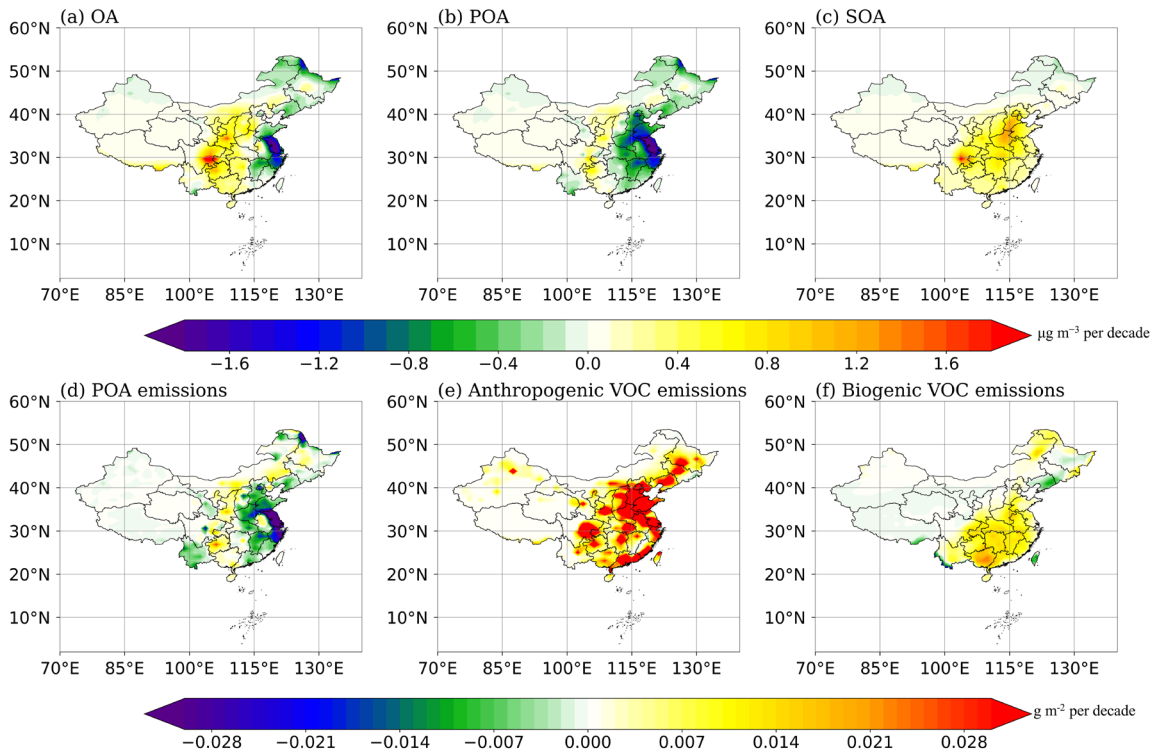
215 Spatial distributions of annual average concentrations of OA and related subspecies are presented in Fig.2. The concentrations of OA show prominent regional differences, with its high values ($>15 \mu\text{g m}^{-3}$) areas concentrated in the North China Plain and Sichuan Basin Area, while the vast remote areas in Western China such as Tibet and Xinjiang show lower OA concentrations ($<5 \mu\text{g m}^{-3}$). Spatial distribution of total OA at national scale is predominantly determined by POA as shown in Fig.2(b). In the densely populated North China Plain urban area, contribution of POA to OA can reach up to 75%. SOA was relatively 220 lower in concentration (Fig.2(c)) and was found to have a consistent spatial distribution pattern as POA, indicating a dominate contribution from anthropogenic VOC derived SOA (ASOA) to total SOA. Spatial distributions of POA and SOA are generally well consistent with anthropogenic POA and VOC emissions which also concentrated over urban clusters as shown in Fig.2(d) and (e) respectively. Pearl River Delta is found to be unique as it has relatively low POA emissions but high anthropogenic VOC emission, probably due to vehicle exhausts (Lee et al., 2002; Liu et al., 2024). It is also important to notice that Southern 225 China has a non-negligible level of SOA where biogenically produced BSOA was found to play an important role due to extensive vegetation coverages with excessive BVOC emissions as shown in Fig.2(f). For example, contributions of BSOA to OA can reach up to 27% over Yunnan-Guizhou Plateau for climatological summer averages.



230 **Figure 2: 1990 to 2019 annual average of surface organic aerosols (OA; a; unit: $\mu\text{g m}^{-3}$), primary organic aerosols (POA; b; unit: $\mu\text{g m}^{-3}$), secondary organic aerosols (SOA; c; unit: $\mu\text{g m}^{-3}$), anthropogenic POA emissions (d; unit: $\text{g m}^{-2} \text{ mon}^{-1}$), anthropogenic volatile organic compounds emissions (e; unit: $\text{g m}^{-2} \text{ mon}^{-1}$), and biogenic volatile organic compounds emissions (f; unit: $\text{g m}^{-2} \text{ mon}^{-1}$) concentrations.**

235 General trends of OA and sub-species were demonstrated in Fig.3, with more details such as time series plots (Fig. S7, S13), trends at seasonal scale (Fig. S16, S17) are presented in supplementary materials. All trends are calculated by linear regression on annual scale over 1990-2019. In general, trend of surface OA concentrations showed a regional difference as decreasing over eastern coastal provinces and increasing over the western inland provinces. For example, the annual average surface OA concentrations showed a significant decreasing trend over Yangtze River Delta by around $-1.4 \mu\text{g m}^{-3}$ per decade (-13.8% per decade). While in Sichuan Basin Area, surface OA shows an increasing trend by $0.4 \mu\text{g m}^{-3}$ per decade (7.3% per decade). Trends in different seasons were consistent with the annual trend mentioned above but with stronger changes, as the increase of OA over Sichuan Basin Area in summer was more prominent, and so did the decrease over Yangtze River Delta in winter (Fig.S16).

240



245

Figure 3: 1990 to 2019 annual average long-term trend of surface organic aerosols (OA; a; unit: $\mu\text{g m}^{-3}$ per decade), primary organic aerosols (POA; b; unit: $\mu\text{g m}^{-3}$ per decade), secondary organic aerosols (SOA; c; unit: $\mu\text{g m}^{-3}$ per decade), primary organic aerosols emissions (d; unit: g m^{-2} per decade), anthropogenic volatile organic compounds emissions (e; unit: g m^{-2} per decade), biogenic volatile organic compounds emissions (f; unit: g m^{-2} per decade).

250

The overall OA trend is the net result of the long-term changes in its sub-species POA (Fig. 3(b)) and SOA (Fig. 3(c)). POA generally showed consistent trends with total OA which decreased in the east by up to -8.9% per decade ($-0.24 \mu\text{g m}^{-3}$ per decade) and increased in the west by up to 13.2% per decade ($0.08 \mu\text{g m}^{-3}$ per decade). SOA showed a clear upward trend throughout the country by 10.8% per decade ($0.16 \mu\text{g m}^{-3}$ per decade). The spatial distributions of the long-term trends of POA and SOA were well consistent with the pattern of changes in emissions as shown in Fig. 3(d-f).

255

It's interesting to notice that the most significant changes in OA were not over the regions with high OA concentrations. The different patterns of changes in POA and SOA lead to various changes of OA over three typical urban cluster areas including North China Plain, Yangtze River Delta, and Sichuan Basin Area. North China Plain has the highest level of total OA but a minor trend, probably due to the net effect of a minor decrease in POA and an increase in ASOA, both driven by changes in anthropogenic emissions. Yangtze River Delta has the lowest level of total OA concentrations but the most significant decreasing trend, primarily due to the reduction of POA. Zheng et al. (2023b) suggested that anthropogenic POA emissions were reduced by -65.7% in Yangtze River Delta over 2005-2019 as a result of air quality management (Zheng et al., 2023b).

Sichuan Basin Area has a relatively high level of OA and also the most significant increasing trend. Changes in emissions suggested that the enhancement was mainly driven by excessive SOA from anthropogenic precursors, as shown in Fig.3(e). A more detailed discussion of anthropogenic and biogenic contributions to this increased SOA over Sichuan Basin Area will be provided in later sections.

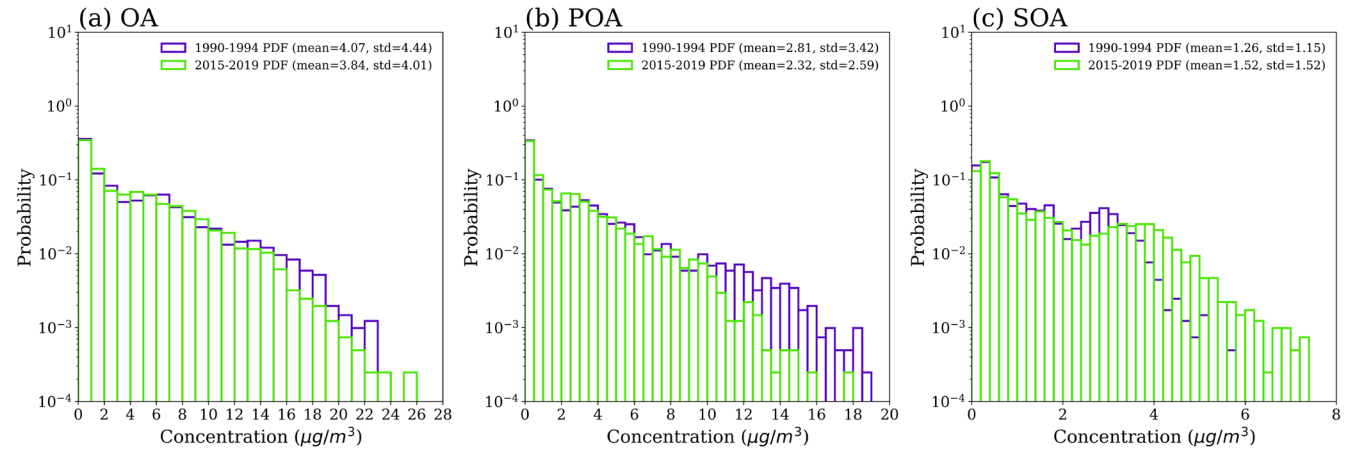


Figure 4: Probability density function (PDF) distributions of simulated five-year average concentrations of surface organic aerosols (OA; a), primary organic aerosols (POA; b), and secondary organic aerosols (SOA; c) for the periods 1990-1994 (purple) and 2015-2019 (green), along with the annual mean values and standard deviations for each species in different time periods.

Given China's vast area, we used probability density function (PDF) to analyze the distribution of OA and its components across different concentration ranges for all grid points, complementing the overall trend analysis. Fig.4(c) shows that the PDF for SOA concentrations flattened out, with higher probability density values, leading to a significant national increase in SOA levels. In contrast, POA trends moved in the opposite direction (Fig.4(b)). While Western China's vast area may impact arithmetic averages, PDF analysis still shows a significant rise in SOA levels, which is consistent with the annual variations calculated using arithmetic averages. To better understand the impact of low OA concentration areas like Xinjiang, Tibet, and Qinghai (Fig.2 (a)), we also analyzed trends while excluding these regions (Table S2). The calculated trends indicate that the impact of low concentration regions is limited, while the overall trend is dominated by changes in high concentration areas.

3.2.1 Attribution of POA trend

We analyzed the decreasing trend of POA and found that both anthropogenic emissions and biomass burning were responsible for it. Anthropogenic emissions contributed 87.4% and dominated the long-term trend, while biomass burning substantially affected the inter-annual variation (IAV) although it only contributed by 12.5% emission on average. As shown in Fig.5(a)

and Fig.S7(a), variations in biomass burning are responsible for the large IAV of POA concentrations. Biomass burning usually has a strong seasonality, so we analyzed its contribution across different seasons (Fig.5(b)). We found that biomass burning in China was most intensive in spring as the relative contribution to total POA emissions was 21.4%. Previous studies have also 290 reported the significant contributions from biomass burning in China, mainly due to agricultural activities. For example, extreme crop residue burning events occurred in Northeast China and Northwest China in 2003 which greatly deteriorated air quality (Wang et al., 2020; Zhuang et al., 2018).

As the largest source of POA, anthropogenic emissions of POA decreased by -7.8% from 1990 to 2019 and is in good 295 agreement with the change of POA concentration. As mentioned in Section 3.3, the change in POA concentration was non-monotonic, which can be explained by the varied changes in anthropogenic POA emissions, as shown in Fig. 5(a). Anthropogenic POA emissions were primarily from residential usage of coal and biofuel (78%), followed by a minor contribution from industry (18%) (Zheng et al., 2018). It increased by 1.6% per year over 1990-2006 along with the expansion 300 of population and Gross Domestic Product (GDP) (Liu et al., 2022; Xing et al., 2022), and then started to gradually decrease by -1.7% per year over 2006-2013 as a result of the emission control policies for industrial sources such as manufacturing 305 boilers (Zheng et al., 2018). Since 2014, China has started to strictly implemented more efficient and national emission control policies which greatly lower the anthropogenic emissions. Policies such as "Action Plan for Air Pollution Prevention and Control" have been reported to play a pivotal role in emission reduction by imposing restrictions on coal use and implementing advanced emission control technologies (Cai et al., 2017; Cui et al., 2020; Feng et al., 2019; Maji et al., 2020). As a result, a 310 rapid reduction of anthropogenic POA emissions started from 2014, which is attributed to broadly replace residential usage of coal and biofuel with electricity and gas. These policies significantly lower the total POA emissions by -42.8% over 2014-2019 (Zheng et al., 2018). Since residential POA emissions were mainly for cooking and heating purposes, we also analyzed the seasonality of anthropogenic POA emissions and found winter indeed showed the greatest contribution (Fig.5(b)). In summary, the changes in POA concentrations and POA emissions during the past 30 years in China could be well explained by the implementation of a series of air pollution management activities.

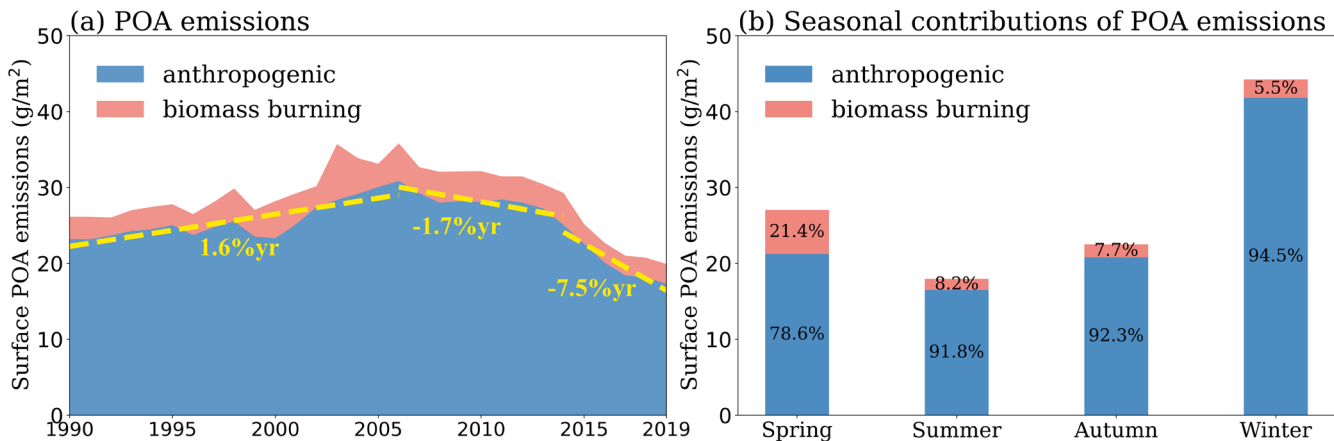
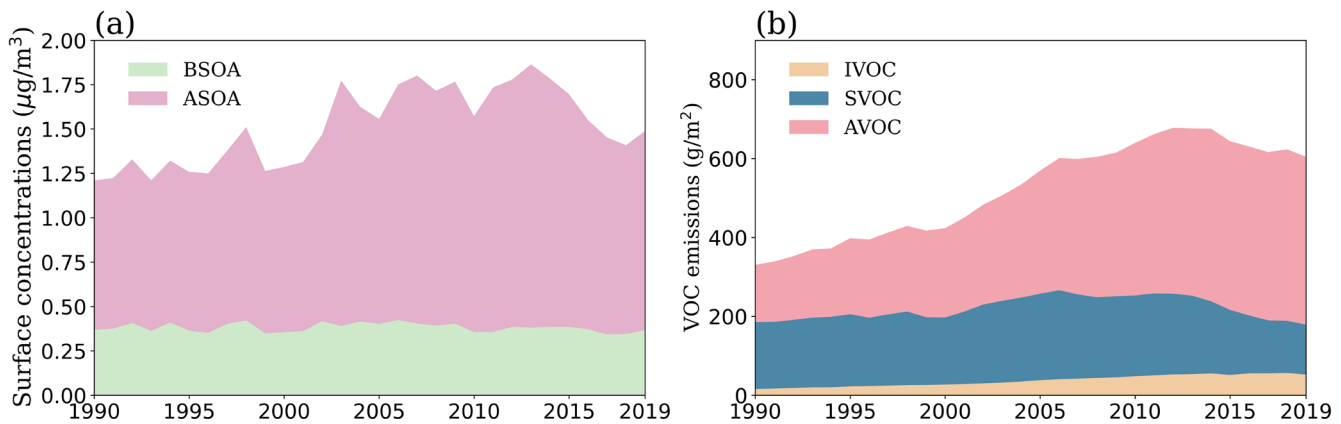


Figure 5: (a) 1990 to 2019 interannual variation of average surface anthropogenic (blue) and biomass burning (pink) primary organic aerosols (POA) emissions (unit: g m⁻² mon⁻¹). The yellow dashed line represents the linear regression fit for anthropogenic POA emissions over the periods 1990–2006, 2006–2014, and 2014–2019. (b) Seasonal average surface anthropogenic (blue) and biomass burning (pink) POA emissions (unit: g m⁻² mon⁻¹) and the relative contribution of different seasons (%).

3.2.2 Attribution of SOA trend

SOA is produced from both anthropogenic and biogenic emissions of VOC. ASOA contributed roughly 74.3% to total SOA during the study period, with high concentrations found over urban areas such as North China Plain, Yangtze River Delta, Sichuan Basin Area, and Pearl River Delta. Anthropogenic VOC mainly consist of aromatics (AVOC), semi-volatile organic compounds (SVOC), and intermediate-volatile organic compounds (IVOC). In contrast to POA, which primarily comes from residential sector, emission sources of anthropogenic VOC are quite complex and have different changes in China over the past decades. AVOC emission is mainly from industry (21%), solvent usage (25%), and transportation (22%) (Zheng et al., 2018). Both industry and solvent usage gradually increased over the past decades and subsequently lead to enhanced AVOC emission although transportation slightly decreased. Anthropogenic AVOC increased by 115.8% from 1990 to 2019, with most significant enhancement over urban clusters mentioned above. Although a prominent decrease of AVOC was observed over 2014–2019, it remains the largest contributor of anthropogenic VOC as shown in Fig. 6(b). IVOC increased throughout the study period (Fig. 7(b)), and their importance in SOA formation grew over time (Fig. S10). However, their relative contribution to total anthropogenic VOC emissions remained minor. SVOC primarily originated from the same sources as POA (Chang et al., 2022). Although SVOC dominated the formation of ASOA in 1990, accounting for 51.9% of the total ASOA (Fig. S10(c)), their concentrations decreased after 2006 due to reduced emissions (Fig. 7(b)). Although SVOC emissions declined, the rise in AVOC emissions not only offset this reduction but also emerged as the primary driver of the sustained increase in ASOA.



335 **Figure 6: (a) Interannual variations in modelled average surface concentrations of secondary organic aerosols from anthropogenic sources (ASOA) and biogenic sources (BSOA) (unit: $\mu\text{g m}^{-3}$). (b) Interannual variations in emissions of aromatics (AVOC), semi-volatile organic compounds (SVOC), and intermediate-volatile organic compounds (IVOC) (unit: $\text{g m}^{-2} \text{ mon}^{-1}$).**

BSOA was found to play an important role especially during summer over South China, and recent studies also revealed that formation of BSOA is closely affected by anthropogenic pollutants such as sulfate and NOx (Liu et al., 2021b; Pye et al., 340 2013). To understand the contribution of BSOA to the long-term trend of total OA over China, we further analyzed the trend of SOA_{IE} and SOA_{MT}, which are the two main components of BSOA. During 1990-2019, SOA_{IE} concentrations decreased by -0.01 $\mu\text{g m}^{-3}$ per decade (-6.3% per decade). The reduction of SOA_{IE} appears to be primarily driven by the combined effect of IEPOX and SO₄²⁻ availability, as the formation mechanism of SOA_{IE} fundamentally relies on the heterogeneous uptake of IEPOX onto sulfate aerosols (Dong et al., 2022; Jo et al., 2019, 2021). On one hand, anthropogenic emission of SO₂ has been 345 greatly lowered by the enforcement of the Energy Conservation and Emission Reduction (ECER) and a corresponding decrease in the concentrations of SO₄²⁻ has been observed (Fig.S18(d)). This is responsible for the decrease in SOA_{IE} since 2006. On the other hand, the precursor IEPOX showed an opposite decreasing trend (Fig.S18(e-f)) as compared to anthropogenic emission enhancement of NOx before 2011, since NOx would affect the oxidation pathway of isoprene. We find a nationwide reduction of SOA_{IE} over the study period, with an exceptional increase in Yunnan province. The increase of SOA_{IE} over 350 Yunnan province shall be due to the combined effect of enhancement in vegetation coverage resulting from ecosystem projects in China (Hua et al., 2018) and the increase of SO₄²⁻ transported from Peninsular Southeast Asia (e.g., Vietnam, Thailand) resulted from development of local industries (Dalsøren et al., 2009; Grandey et al., 2018). In summary, our results suggested that the change in SOA_{IE} is affected by SO₄²⁻, which is consistent with previous studies using different models (Liu et al., 2021b; Qin et al., 2018).

355

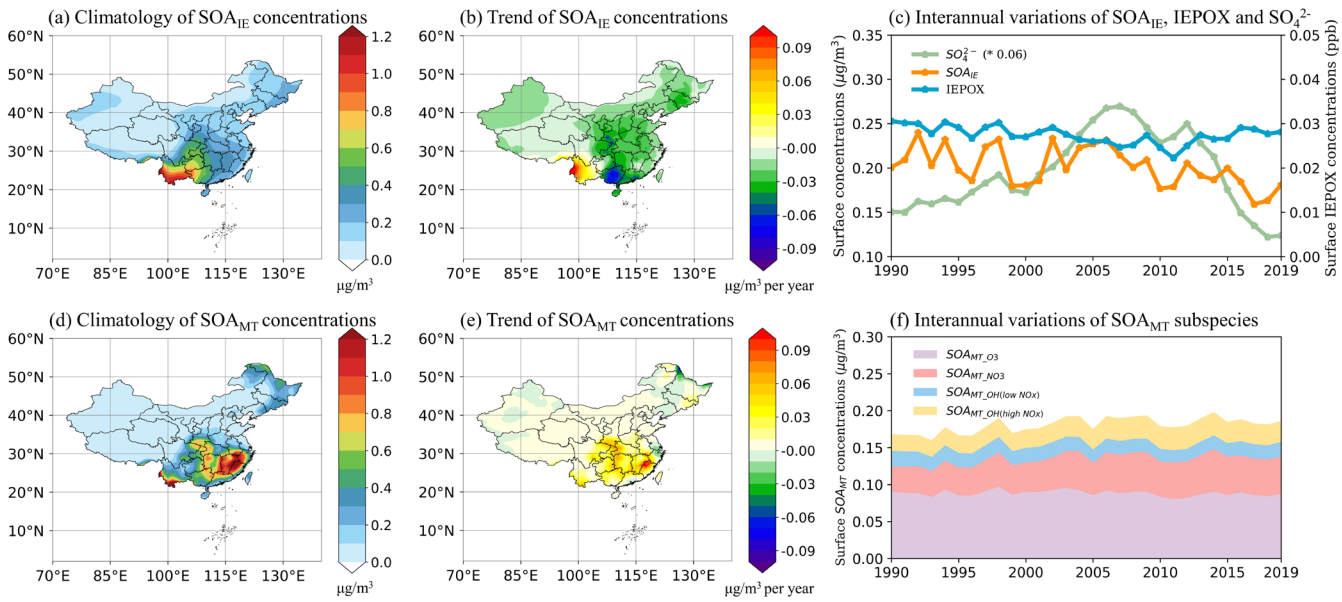


Figure 7: (a) 1990 to 2019 annual average of surface SOA_{IE} (isoprene-epoxydiol-derived secondary organic aerosols; unit: $\mu\text{g m}^{-3}$) concentrations. (b) 1990 to 2019 annual average long-term trend of surface SOA_{IE} (unit: $\mu\text{g m}^{-3}$ per decade) concentrations. (c) Interannual variations of average surface SOA_{IE} (left Y axis), IEPOX (isoprene epoxydiol; right Y axis) and SO_4^{2-} (scaled by a factor of 0.06; left Y axis) concentrations during 1990-2019. (d) 1990 to 2019 annual average of surface SOA_{MT} (monoterpene-derived secondary organic aerosols; unit: $\mu\text{g m}^{-3}$) concentrations. (e) 1990 to 2019 annual average long-term trend of surface SOA_{MT} (unit: $\mu\text{g m}^{-3}$ per decade) concentrations. (f) Interannual variations of average surface SOA_{MT} subspecies concentrations during 1990-2019 (unit: $\mu\text{g m}^{-3}$).

360

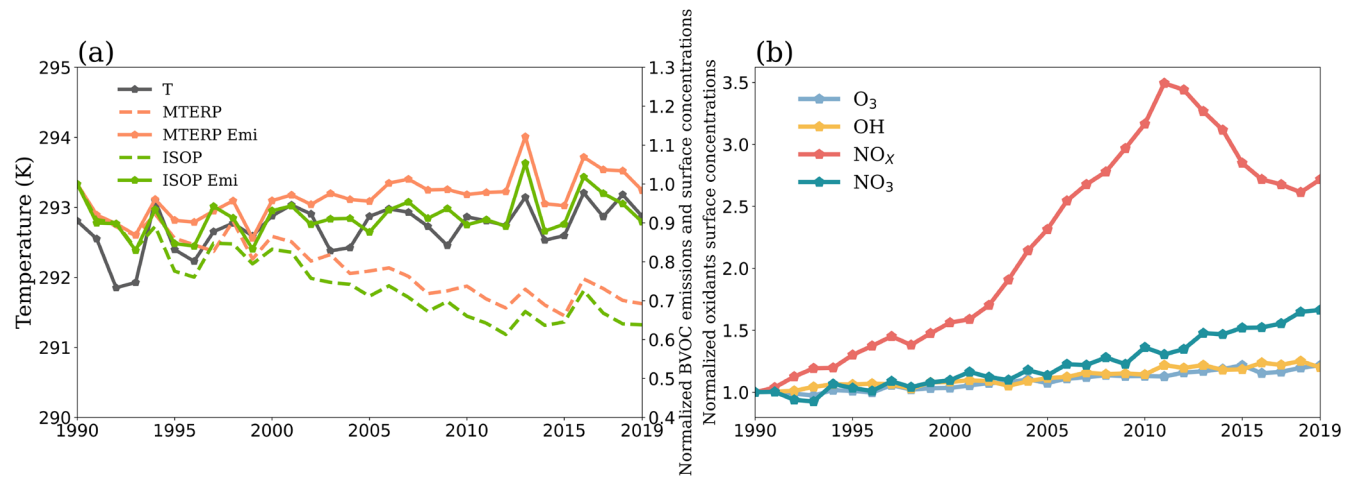
365 Monoterpene-derived SOA was sensitive to both NOx level and biogenic emission, so we first analyzed the trend of SOA_{MT} and its subspecies and then employed sensitivity simulations to distinguish the influences from chemistry and emission. Monoterpenes can be oxidized by different oxidants to form SOA_{MT} , so the change in anthropogenic NOx emission may affect the trend of SOA_{MT} by altering the oxidation pathways. We found in the long-term simulation that the net effect of different oxidation pathways led to an overall increasing trend of SOA_{MT} , as shown in Fig.7(e-f). We defined four subspecies of SOA_{MT} :

370 $\text{SOA}_{\text{MT}, \text{O}_3}$, $\text{SOA}_{\text{MT}, \text{NO}_3}$, $\text{SOA}_{\text{MT}, \text{OH}(\text{low NO}_x)}$, and $\text{SOA}_{\text{MT}, \text{OH}(\text{high NO}_x)}$, which are produced from O_3 oxidation, nitrate radical (NO_3) oxidation, hydroxyl radical (OH) oxidation under low NOx condition and OH oxidation under high NOx condition, respectively. The main contributor to SOA_{MT} concentration in China was $\text{SOA}_{\text{MT}, \text{O}_3}$ (34.6%, Fig.S19(a)), followed by $\text{SOA}_{\text{MT}, \text{NO}_3}$ (31.2%, Fig.S19(c)), $\text{SOA}_{\text{MT}, \text{OH}(\text{high NO}_x)}$ (18.1%, Fig.S19(g)) and $\text{SOA}_{\text{MT}, \text{OH}(\text{low NO}_x)}$ (16.1%, Fig.S19(e)). The different SOA_{MT} components had regionally different or even opposite long-term trends. $\text{SOA}_{\text{MT}, \text{NO}_3}$ showed a regionally consistent and significant increasing trend (Fig.S19(d)) in line with SOA_{MT} (4.1% per decade) (Fig.7(e)). A slight but solid increasing trend in $\text{SOA}_{\text{MT}, \text{OH}(\text{high NO}_x)}$ is shown in Fig.S19(h), which together with the enhancement of $\text{SOA}_{\text{MT}, \text{NO}_3}$

375

concentrations dominates the increasing trend in total SOA_{MT} . $\text{SOA}_{\text{MT-O}_3}$ (Fig.S19(b)) and $\text{SOA}_{\text{MT-OH}(\text{low NO}_x)}$ (Fig.S19(f)) had similar trends but the change in $\text{SOA}_{\text{MT-OH}(\text{low NO}_x)}$ was relatively smaller.

380 The decreasing trend in $\text{SOA}_{\text{MT-O}_3}$ and $\text{SOA}_{\text{MT-OH}(\text{low NO}_x)}$ offset the enhancement in the other two SOA_{MT} components. The different trends of SOA_{MT} components were affected by the changes in oxidants, which were mainly determined by changes in anthropogenic NO_x emissions (Fig.8(b)). The surface concentrations of NO_x and NO₃ increased over 1990–2019, while O₃ and OH increased relatively slowly, which led to differences in the variation of the SOA_{MT} components during the study period. 385 The total SOA_{MT} has increased since 1990 primarily due to increased monoterpenes emissions because of both a higher temperature (Fig.8(a)) and also enhanced vegetation coverage (Guenther et al., 2012; Fu and Liao, 2014). Related studies suggested that vegetation coverage was increase over China during the past due to a series of ecological restoration and 390 conservation policies (Guo et al., 2022), such as the Grain-for-Green Program (Yin et al., 2018) and Urban Ecological Civilization Construction. These policies have effectively promoted vegetation recovery and expansion, while also driving the continuous increase in urban greening areas. These changes collectively contributed to the rising trend in BVOC emissions and subsequent changes in SOA concentrations.

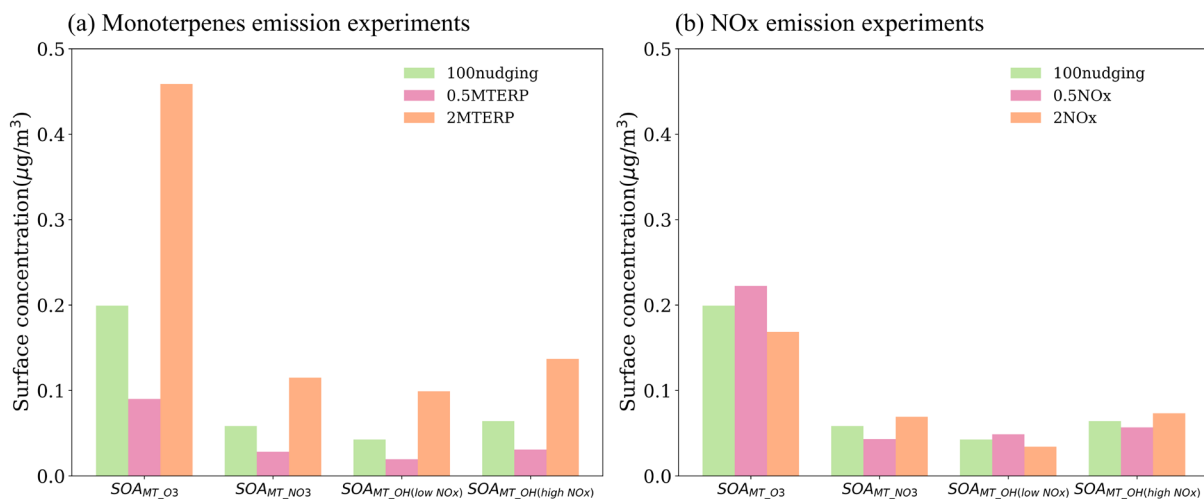


395 **Figure 8: (a) 1990 to 2019 JJA time series of surface temperature (dark gray solid line; left Y axis; unit: K), relative changing ratio of surface concentrations for monoterpenes (orange dashed line; right Y axis; MTERP), isoprene (green dashed line; right Y axis; ISOP), monoterpenes emissions (orange solid line; right Y axis; MTERP Emi) and isoprene emissions (green solid line; right Y axis; ISOP Emi). (b) 1990 to 2019 JJA time series of relative changing ratio of surface concentrations for nitrogen oxidants (NO_x; red), ozone (O₃; pale blue), hydroxyl radical (OH; yellow), and nitrate radical (NO₃; cyan). All relative changing ratios are calculated as the concentration in each year divided by the concentration in 1990.**

400 Since anthropogenic NO_x emission change may have a nonlinear effect on SOA_{MT} , we applied sensitivity simulations by perturbing NO_x emissions and biogenic emissions respectively to quantify their contributions. We found that the response of

SOA_{MT} to NOx emission change was almost negligible when NOx emissions rose to twice the 100nudging or fell to half the 100nudging in July 2013 (Fig.9(b)), although the major atmospheric oxidizers such as O₃, OH, NO₃, and NOx showed significant changes (Fig.S22). For example, the increase in NOx emissions drove SOA_{MT_OH(high NOx)} and SOA_{MT_NO3} to increase, 405 but meanwhile, the effect was offset by decreases in SOA_{MT_OH(low NOx)} and SOA_{MT_O3}. Similarly, under condition of NOx emission reduction, the SOA_{MT} response was small due to the offsetting relative changes in the SOA_{MT} components. Our simulation results suggested that anthropogenic emission change has a very limited net effect on SOA_{MT} over the study period.

Through sensitivity simulations by perturbing monoterpenes emission, however, we found that the responses of SOA_{MT} and 410 its components were almost linear. When the monoterpenes emissions increased to twice that of the 100nudging in July 2013, the concentrations of SOA_{MT} and its components on the surface of China also increased by two times. Meanwhile, when the monoterpenes emission decreased to half of the 100nudging, the concentrations of SOA_{MT} and its components decreased by half too (Fig.9(a)). Changes in monoterpenes emissions showed a minor impact on atmospheric oxidants (Fig.S25). In brief summary, we found that anthropogenic NOx emission change has a very limited impact on SOA_{MT}, while enhanced 415 monoterpenes emissions due to a warmer surface temperature dominate the increasing trend over 1990-2019.



420 **Figure 9: Surface concentrations (unit: $\mu\text{g m}^{-3}$) of monoterpane-derived secondary organic aerosols (SOA_{MT}) compositions for July 2013 from the monoterpenes (a) and NOx (b) sensitivity experiments named 100nudging (green bar), 0.5MTERP/NOx (pink bar), and 2MTERP/NOx (orange bar).**

4. Summary and discussion

In this study we applied the CAM-chem model along with ground-based measurements and the CAQRA-aerosols dataset to investigate the long-term trend of OA in 1990-2019 in China. A slight increase of total OA by 1.8% per decade was found to

be a net effect of decrease in POA by $-0.08 \mu\text{g m}^{-3}$ per decade (-2.7% per decade) and enhancement of SOA by $0.16 \mu\text{g m}^{-3}$ per decade (10.8% per decade). There are significant regional differences in the change trend of OA, which generally decreased in the east (e.g., Yangtze River Delta) and increased in the west (e.g., Sichuan Basin), and this trend was more significant in winter, indicating the dominant contribution from primary anthropogenic emission of POA.

Further analyzing the causes of POA and SOA trends, we found that the main factors affecting POA trends are biomass burning and anthropogenic emissions. Anthropogenic emissions accounted for 87.4% and dominated the long-term trend of POA, but biomass burning dominated the IAV. We found that anthropogenic VOC made a major contribution to total SOA by 74.3% and the spatiotemporal characteristics were well consistent with POA. For SOA produced from BVOC, we found in the simulation that BSOA plays an important role over South China especially in summer with contribution up to 47.1%. Total BSOA decreased by -4.1% over the study period. Isoprene derived SOA_{IE} is greatly affected by heterogeneous reactions catalyzed by sulfate, which decreased rapidly since 2006 and resulted in a decline by -18.8% over 1990-2019. On the other hand, monoterpene-derived SOA_{MT} increased by 12.3%. We found through sensitivity experiments that anthropogenic NO_x emissions change had an almost negligible impact on total SOA_{MT}, although the contributions from different oxidation pathways changed slightly. The trend in SOA_{MT} was dominated by increased biological emissions due to a warmer climate.

Our study revealed the change of total OA in China during the past 30 years and the contribution from various driving factors. Anthropogenic emission, biomass burning emission, and biogenic emission all showed important and unique impacts on the long-term trend of OA, indicating that future air quality management would be recommended to take a comprehensive consideration of the abovementioned sources. Especially, we found that anthropogenic contributions to both POA and SOA substantially decreased since 2014, while biogenic contribution has the potential to increase under a warming climate. BSOA plays a minor role on a national scale but may have significant contribution over densely vegetated southern areas of China during summer, while a main part of it is hardly affected by anthropogenic emissions but is enhanced by a warming climate. This implies that future research may need to pay more attention to biogenic sources. In addition, it should be noticed that our current model may have deficiencies in terms of both emission inventory and chemical mechanism for simulating SOA. For example, current model only considers the heterogeneous production of IEPOX derived SOA, but recent studies show that isoprene may also produce SOA through intermediate oxidation gas-phase products hydroxymethylmethyl- α -lactone (HMML) and methacrylic acid epoxide (MAE) (He et al., 2018; Zhang, 2023), which are not considered in the current model. This may also be partially responsible for the underestimation of SOA mentioned earlier. Therefore, continuous development of the SOA chemical mechanisms is recommended to improve the simulation capability of the model. And in addition, more detailed observations of OA components are needed to further investigate the interactions between biological and anthropogenic sources.

Data availability. The long-term CAM6-Chem model data is too large to be published through public FTP or cloud drives. It will be made available upon reasonable request. Ground-based measurements for OA, POA, and SOA were obtained from the supplementary materials of published articles by Miao et al. (2021) and Chen et al. (2024). The publicly available high-resolution simulation dataset of PM_{2.5} composition over China (CAQRA-aerosols) was obtained from the Data Integration Project of the National Natural Science Foundation's Air Pollution Complex Major Research Plan (Project Number: 92044303) via the China Air Pollution Data Center (CAPDC) (<https://www.capdatabase.cn>). The 24-hour average PM_{2.5} and O₃ data can be accessed from the China Environmental Monitoring Terminal (CEMT) National Urban Air Quality Real-Time Distribution Platform (NUAQRPD) (<https://air.cnemc.cn:18007/>). MODIS AOD data is available at <https://atmosphere-imager.gsfc.nasa.gov/products/aerosol>. NO₂ column concentration data can be accessed from the OMI (Ozone Monitoring Instrument) Level-3 dataset on NASA's AURA satellite platform (<https://disc.gsfc.nasa.gov/datasets?keywords=OMI&page=1>).

Author contributions. MW and XD designed the study. WZ performed the data analysis, produced the figures, and wrote the manuscript draft. YL and MY contributed to the model simulations. All the authors contributed to the discussion and editing of the manuscript.

Competing interests. At least one of the (co-)authors is a member of the editorial board of Atmospheric Chemistry and Physics.

Acknowledgments. This work is supported by the National Natural Science Foundation of China (grant numbers 41925023, 42075102, and 42361144711), and the Fundamental Research Funds for the Central Universities - CEMAC “GeoX” Interdisciplinary Program (2024ZD05) by the Frontiers Science Center for Critical Earth Material Cycling, Nanjing University. We greatly thank the High Performance Computing Center (HPCC) of Nanjing University for providing the computational resources used in this work. We also thank the Tsinghua University group for providing the MEIC emission used in our simulations. The CESM project is supported primarily by the U.S. National Science Foundation.

References

An, Z., Huang, R.-J., Zhang, R., Tie, X., Li, G., Cao, J., Zhou, W., Shi, Z., Han, Y., Gu, Z., and Ji, Y.: Severe haze in northern China: A synergy of anthropogenic emissions and atmospheric processes, Proc. Natl. Acad. Sci., 116, 8657–8666, <https://doi.org/10.1073/pnas.1900125116>, 2019.

Cai, S., Wang, Y., Zhao, B., Wang, S., Chang, X., and Hao, J.: The impact of the “Air Pollution Prevention and Control Action Plan” on PM_{2.5} concentrations in Jing-Jin-Ji region during 2012–2020, Sci. Total Environ., 580, 197–209, <https://doi.org/10.1016/j.scitotenv.2016.11.188>, 2017.

Chang, X., Zhao, B., Zheng, H., Wang, S., Cai, S., Guo, F., Gui, P., Huang, G., Wu, D., Han, L., Xing, J., Man, H., Hu, R., Liang, C., Xu, Q., Qiu, X., Ding, D., Liu, K., Han, R., Robinson, A. L., and Donahue, N. M.: Full-volatility emission framework corrects missing and underestimated secondary organic aerosol sources, *One Earth*, 5, 403–412, <https://doi.org/10.1016/j.oneear.2022.03.015>, 2022.

Chen, Q., Miao, R., Geng, G., Shrivastava, M., Dao, X., Xu, B., Sun, J., Zhang, X., Liu, M., Tang, G., Tang, Q., Hu, H., Huang, R.-J., Wang, H., Zheng, Y., Qin, Y., Guo, S., Hu, M., and Zhu, T.: Widespread 2013–2020 decreases and reduction challenges of organic aerosol in China, *Nat. Commun.*, 15, 4465, <https://doi.org/10.1038/s41467-024-48902-0>, 2024.

Cui, L., Zhou, J., Peng, X., Ruan, S., and Zhang, Y.: Analyses of air pollution control measures and co-benefits in the heavily air-polluted Jinan city of China, 2013–2017, *Sci. Rep.*, 10, 5423, <https://doi.org/10.1038/s41598-020-62475-0>, 2020.

Dalsøren, S. B., Isaksen, I. S. A., Li, L., and Richter, A.: Effect of emission changes in Southeast Asia on global hydroxyl and methane lifetime, *Tellus B Chem. Phys. Meteorol.*, 61, 588, <https://doi.org/10.1111/j.1600-0889.2009.00429.x>, 2009.

Ding, X., Zhang, Y., He, Q., Yu, Q., Shen, R., Zhang, Y., Zhang, Z., Lyu, S., Hu, Q., Wang, Y., Li, L., Song, W., and Wang, X.: Spatial and seasonal variations of secondary organic aerosol from terpenoids over China, *J. Geophys. Res. Atmospheres*, 121, <https://doi.org/10.1002/2016JD025467>, 2016.

Donahue, N. M., Robinson, A. L., Stanier, C. O., and Pandis, S. N.: Coupled Partitioning, Dilution, and Chemical Aging of Semivolatile Organics, *Environ. Sci. Technol.*, 40, 2635–2643, <https://doi.org/10.1021/es052297c>, 2006.

Dong, X., Liu, Y., Li, X., Yue, M., Liu, Y., Ma, Z., Zheng, H., Huang, R., and Wang, M.: Modeling Analysis of Biogenic Secondary Organic Aerosol Dependence on Anthropogenic Emissions in China, *Environ. Sci. Technol. Lett.*, 9, 286–292, <https://doi.org/10.1021/acs.estlett.2c00104>, 2022.

Emmons, L. K., Schwantes, R. H., Orlando, J. J., Tyndall, G., Kinnison, D., Lamarque, J., Marsh, D., Mills, M. J., Tilmes, S., Bardeen, C., Buchholz, R. R., Conley, A., Gettelman, A., Garcia, R., Simpson, I., Blake, D. R., Meinardi, S., and Pétron, G.: The Chemistry Mechanism in the Community Earth System Model Version 2 (CESM2), *J. Adv. Model. Earth Syst.*, 12, e2019MS001882, <https://doi.org/10.1029/2019MS001882>, 2020.

Fadel, M., Ledoux, F., Farhat, M., Kfouri, A., Courcot, D., and Afif, C.: PM2.5 characterization of primary and secondary organic aerosols in two urban-industrial areas in the East Mediterranean, *J. Environ. Sci.*, 101, 98–116, <https://doi.org/10.1016/j.jes.2020.07.030>, 2021.

Fan, Y., Liu, C.-Q., Li, L., Ren, L., Ren, H., Zhang, Z., Li, Q., Wang, S., Hu, W., Deng, J., Wu, L., Zhong, S., Zhao, Y., Pavuluri, C. M., Li, X., Pan, X., Sun, Y., Wang, Z., Kawamura, K., Shi, Z., and Fu, P.: Large contributions of biogenic and anthropogenic sources to fine organic aerosols in Tianjin, North China, *Atmospheric Chem. Phys.*, 20, 117–137, <https://doi.org/10.5194/acp-20-117-2020>, 2020.

Feng, Y., Ning, M., Lei, Y., Sun, Y., Liu, W., and Wang, J.: Defending blue sky in China: Effectiveness of the “Air Pollution Prevention and Control Action Plan” on air quality improvements from 2013 to 2017, *J. Environ. Manage.*, 252, 109603, <https://doi.org/10.1016/j.jenvman.2019.109603>, 2019.

Gelaro, R., McCarty, W., Suárez, M. J., Todling, R., Molod, A., Takacs, L., Randles, C. A., Darmenov, A., Bosilovich, M. G., Reichle, R., Wargan, K., Coy, L., Cullather, R., Draper, C., Akella, S., Buchard, V., Conaty, A., Da Silva, A. M., Gu, W., Kim, G.-K., Koster, R., Lucchesi, R., Merkova, D., Nielsen, J. E., Partyka, G., Pawson, S., Putman, W., Rienecker, M., Schubert, S. D., Sienkiewicz, M., and Zhao, B.: The Modern-Era Retrospective Analysis for Research and Applications, Version 2 (MERRA-2), *J. Clim.*, 30, 5419–5454, <https://doi.org/10.1175/JCLI-D-16-0758.1>, 2017.

525 Gettelman, A. and Morrison, H.: Advanced Two-Moment Bulk Microphysics for Global Models. Part I: Off-Line Tests and Comparison with Other Schemes, *J. Clim.*, 28, 1268–1287, <https://doi.org/10.1175/JCLI-D-14-00102.1>, 2015.

Grandey, B. S., Yeo, L. K., Lee, H., and Wang, C.: The Equilibrium Climate Response to Sulfur Dioxide and Carbonaceous Aerosol Emissions From East and Southeast Asia, *Geophys. Res. Lett.*, 45, <https://doi.org/10.1029/2018GL080127>, 2018.

530 Guenther, A. B., Jiang, X., Heald, C. L., Sakulyanontvittaya, T., Duhl, T., Emmons, L. K., and Wang, X.: The Model of Emissions of Gases and Aerosols from Nature version 2.1 (MEGAN2.1): an extended and updated framework for modeling biogenic emissions, *Geosci. Model Dev.*, 5, 1471–1492, <https://doi.org/10.5194/gmd-5-1471-2012>, 2012.

Guo, J., Gong, P., Dronova, I., and Zhu, Z.: Forest cover change in China from 2000 to 2016, *Int. J. Remote Sens.*, 43, 593–606, <https://doi.org/10.1080/01431161.2021.2022804>, 2022.

535 Hallquist, M., Wenger, J. C., Baltensperger, U., Rudich, Y., Simpson, D., Claeys, M., Dommen, J., Donahue, N. M., George, C., Goldstein, A. H., Hamilton, J. F., Herrmann, H., Hoffmann, T., Iinuma, Y., Jang, M., Jenkin, M. E., Jimenez, J. L., Kiendler-Scharr, A., Maenhaut, W., McFiggans, G., Mentel, T. F., Monod, A., Prevot, A. S. H., Seinfeld, J. H., Surratt, J. D., Szmigielski, R., and Wildt, J.: The formation, properties and impact of secondary organic aerosol: current and emerging issues, *Atmos. Chem. Phys.*, 2009.

540 He, Q., Ding, X., Fu, X., Zhang, Y., Wang, J., Liu, Y., Tang, M., Wang, X., and Rudich, Y.: Secondary Organic Aerosol Formation From Isoprene Epoxides in the Pearl River Delta, South China: IEPOX- and HMML-Derived Tracers, *J. Geophys. Res. Atmospheres*, 123, 6999–7012, <https://doi.org/10.1029/2017JD028242>, 2018.

Hodzic, A., Kasibhatla, P. S., Jo, D. S., Cappa, C. D., Jimenez, J. L., Madronich, S., and Park, R. J.: Rethinking the global secondary organic aerosol (SOA) budget: stronger production, faster removal, shorter lifetime, *Atmospheric Chem. Phys.*, 16, 545 7917–7941, <https://doi.org/10.5194/acp-16-7917-2016>, 2016.

Hoyle, C. R., Boy, M., Donahue, N. M., Fry, J. L., Glasius, M., Guenther, A., Hallar, A. G., Huff Hartz, K., Petters, M. D., Petäjä, T., Rosenoern, T., and Sullivan, A. P.: A review of the anthropogenic influence on biogenic secondary organic aerosol, *Atmospheric Chem. Phys.*, 11, 321–343, <https://doi.org/10.5194/acp-11-321-2011>, 2011.

Hu, J., Wang, P., Ying, Q., Zhang, H., Chen, J., Ge, X., Li, X., Jiang, J., Wang, S., Zhang, J., Zhao, Y., and Zhang, Y.: 550 Modeling biogenic and anthropogenic secondary organic aerosol in China, *Atmospheric Chem. Phys.*, 17, 77–92, <https://doi.org/10.5194/acp-17-77-2017>, 2017.

Hua, F., Wang, L., Fisher, B., Zheng, X., Wang, X., Yu, D. W., Tang, Y., Zhu, J., and Wilcove, D. S.: Tree plantations displacing native forests: The nature and drivers of apparent forest recovery on former croplands in Southwestern China from 2000 to 2015, *Biol. Conserv.*, 222, 113–124, <https://doi.org/10.1016/j.biocon.2018.03.034>, 2018.

555 Huang, R.-J., Wang, Y., Cao, J., Lin, C., Duan, J., Chen, Q., Li, Y., Gu, Y., Yan, J., Xu, W., Fröhlich, R., Canonaco, F., Bozzetti, C., Ovadnevaite, J., Ceburnis, D., Canagaratna, M. R., Jayne, J., Worsnop, D. R., El-Haddad, I., Prévôt, A. S. H., and O'Dowd, C. D.: Primary emissions versus secondary formation of fine particulate matter in the most polluted city (Shijiazhuang) in North China, *Atmospheric Chem. Phys.*, 19, 2283–2298, <https://doi.org/10.5194/acp-19-2283-2019>, 2019.

560 Jo, D. S., Hodzic, A., Emmons, L. K., Marais, E. A., Peng, Z., Nault, B. A., Hu, W., Campuzano-Jost, P., and Jimenez, J. L.: A simplified parameterization of isoprene-epoxydiol-derived secondary organic aerosol (IEPOX-SOA) for global chemistry and climate models: a case study with GEOS-Chem v11-02-rc, *Geosci. Model Dev.*, 12, 2983–3000, <https://doi.org/10.5194/gmd-12-2983-2019>, 2019.

565 Jo, D. S., Hodzic, A., Emmons, L. K., Tilmes, S., Schwantes, R. H., Mills, M. J., Campuzano-Jost, P., Hu, W., Zaveri, R. A., Easter, R. C., Singh, B., Lu, Z., Schulz, C., Schneider, J., Shilling, J. E., Wisthaler, A., and Jimenez, J. L.: Future changes in isoprene-epoxydiol-derived secondary organic aerosol (IEPOX SOA) under the Shared Socioeconomic Pathways: the importance of physicochemical dependency, *Atmospheric Chem. Phys.*, 21, 3395–3425, <https://doi.org/10.5194/acp-21-3395-2021>, 2021.

570 Kanellopoulos, P. G., Verouti, E., Chrysochou, E., Koukoulakis, K., and Bakeas, E.: Primary and secondary organic aerosol in an urban/industrial site: Sources, health implications and the role of plastic enriched waste burning, *J. Environ. Sci.*, 99, 222–238, <https://doi.org/10.1016/j.jes.2020.06.012>, 2021.

Kong, L., Tang, X., Zhu, J., Wang, Z., Li, J., Wu, H., Wu, Q., Chen, H., Zhu, L., Wang, W., Liu, B., Wang, Q., Chen, D., Pan, Y., Song, T., Li, F., Zheng, H., Jia, G., Lu, M., Wu, L., and Carmichael, G. R.: A 6-year-long (2013–2018) high-resolution air quality reanalysis dataset in China based on the assimilation of surface observations from CNEMC, *Earth Syst. Sci. Data*, 13, 529–570, <https://doi.org/10.5194/essd-13-529-2021>, 2021.

575 Lee, S. C., Chiu, M. Y., Ho, K. F., Zou, S. C., and Wang, X.: Volatile organic compounds (VOCs) in urban atmosphere of Hong Kong, *Chemosphere*, 48, 375–382, [https://doi.org/10.1016/S0045-6535\(02\)00040-1](https://doi.org/10.1016/S0045-6535(02)00040-1), 2002.

Levy, R. C., Mattoo, S., Munchak, L. A., Remer, L. A., Sayer, A. M., Patadia, F., and Hsu, N. C.: The Collection 6 MODIS aerosol products over land and ocean, *Atmospheric Meas. Tech.*, 6, 2989–3034, <https://doi.org/10.5194/amt-6-2989-2013>, 2013.

580 Li, M., Liu, H., Geng, G., Hong, C., Liu, F., Song, Y., Tong, D., Zheng, B., Cui, H., Man, H., Zhang, Q., and He, K.: Anthropogenic emission inventories in China: a review, *Natl. Sci. Rev.*, 4, 834–866, <https://doi.org/10.1093/nsr/nwx150>, 2017.

Lin, C. Q., Liu, G., Lau, A. K. H., Li, Y., Li, C. C., Fung, J. C. H., and Lao, X. Q.: High-resolution satellite remote sensing of provincial PM2.5 trends in China from 2001 to 2015, *Atmos. Environ.*, 180, 110–116, <https://doi.org/10.1016/j.atmosenv.2018.02.045>, 2018.

585 Liu, G., Ma, X., Li, W., Chen, J., Ji, Y., and An, T.: Pollution characteristics, source appointment and environmental effect of oxygenated volatile organic compounds in Guangdong-Hong Kong-Macao Greater Bay Area: Implication for air quality management, *Sci. Total Environ.*, 919, 170836, <https://doi.org/10.1016/j.scitotenv.2024.170836>, 2024.

Liu, P., Zhou, H., Chun, X., Wan, Z., Liu, T., Sun, B., Wang, J., and Zhang, W.: Characteristics of fine carbonaceous aerosols in Wuhai, a resource-based city in Northern China: Insights from energy efficiency and population density, *Environ. Pollut.*, 292, 118368, <https://doi.org/10.1016/j.envpol.2021.118368>, 2022.

590

Liu, X., Ma, P.-L., Wang, H., Tilmes, S., Singh, B., Easter, R. C., Ghan, S. J., and Rasch, P. J.: Description and evaluation of a new four-mode version of the Modal Aerosol Module (MAM4) within version 5.3 of the Community Atmosphere Model, *Geosci. Model Dev.*, 9, 505–522, <https://doi.org/10.5194/gmd-9-505-2016>, 2016.

Liu, Y., Dong, X., Wang, M., Emmons, L. K., Liu, Y., Liang, Y., Li, X., and Shrivastava, M.: Analysis of secondary organic 595 aerosol simulation bias in the Community Earth System Model (CESM2.1), *Atmospheric Chem. Phys.*, 21, 8003–8021, <https://doi.org/10.5194/acp-21-8003-2021>, 2021a.

Liu, Y., Liu, Y., Wang, M., Dong, X., Zheng, Y., Shrivastava, M., Qian, Y., Bai, H., Li, X., and Yang, X.-Q.: Anthropogenic– 600 biogenic interaction amplifies warming from emission reduction over the southeastern US, *Environ. Res. Lett.*, 16, 124046, <https://doi.org/10.1088/1748-9326/ac3285>, 2021b.

Liu, Y., Dong, X., Emmons, L. K., Jo, D. S., Liu, Y., Shrivastava, M., Yue, M., Liang, Y., Song, Z., He, X., and Wang, M.: Exploring the Factors Controlling the Long-Term Trend (1988–2019) of Surface Organic Aerosols in the Continental United 605 States by Simulations, *J. Geophys. Res. Atmospheres*, 128, e2022JD037935, <https://doi.org/10.1029/2022JD037935>, 2023.

Lu, X., Zhang, S., Xing, J., Wang, Y., Chen, W., Ding, D., Wu, Y., Wang, S., Duan, L., and Hao, J.: Progress of Air Pollution Control in China and Its Challenges and Opportunities in the Ecological Civilization Era, *Engineering*, 6, 1423–1431, <https://doi.org/10.1016/j.eng.2020.03.014>, 2020.

610

Ma, Z., Hu, X., Sayer, A. M., Levy, R., Zhang, Q., Xue, Y., Tong, S., Bi, J., Huang, L., and Liu, Y.: Satellite-Based Spatiotemporal Trends in PM_{2.5} Concentrations: China, 2004–2013, *Environ. Health Perspect.*, 124, 184–192, <https://doi.org/10.1289/ehp.1409481>, 2016.

Maji, K. J., Li, V. Ok., and Lam, J. Ck.: Effects of China's current Air Pollution Prevention and Control Action Plan on air 615 pollution patterns, health risks and mortalities in Beijing 2014–2018, *Chemosphere*, 260, 127572, <https://doi.org/10.1016/j.chemosphere.2020.127572>, 2020.

Malm, W. C. and Hand, J. L.: An examination of the physical and optical properties of aerosols collected in the IMPROVE program, *Atmos. Environ.*, 41, 3407–3427, <https://doi.org/10.1016/j.atmosenv.2006.12.012>, 2007.

Miao, R., Chen, Q., Shrivastava, M., Chen, Y., Zhang, L., Hu, J., Zheng, Y., and Liao, K.: Process-based and observation- 620 constrained SOA simulations in China: the role of semivolatile and intermediate-volatility organic compounds and OH levels, *Atmospheric Chem. Phys.*, 21, 16183–16201, <https://doi.org/10.5194/acp-21-16183-2021>, 2021.

Pye, H. O. T., Pinder, R. W., Piletic, I. R., Xie, Y., Capps, S. L., Lin, Y.-H., Surratt, J. D., Zhang, Z., Gold, A., Luecken, D. J., Hutzell, W. T., Jaoui, M., Offenberg, J. H., Kleindienst, T. E., Lewandowski, M., and Edney, E. O.: Epoxide Pathways Improve Model Predictions of Isoprene Markers and Reveal Key Role of Acidity in Aerosol Formation, *Environ. Sci. Technol.*, 47, 11056–11064, <https://doi.org/10.1021/es402106h>, 2013.

Pye, H. O. T., D'Ambro, E. L., Lee, B. H., Schobesberger, S., Takeuchi, M., Zhao, Y., Lopez-Hilfiker, F., Liu, J., Shilling, J. E., Xing, J., Mathur, R., Middlebrook, A. M., Liao, J., Welti, A., Graus, M., Warneke, C., De Gouw, J. A., Holloway, J. S., Ryerson, T. B., Pollack, I. B., and Thornton, J. A.: Anthropogenic enhancements to production of highly oxygenated molecules from autoxidation, *Proc. Natl. Acad. Sci.*, 116, 6641–6646, <https://doi.org/10.1073/pnas.1810774116>, 2019.

625 Qin, M., Wang, X., Hu, Y., Ding, X., Song, Y., Li, M., Vasilakos, P., Nenes, A., and Russell, A. G.: Simulating Biogenic Secondary Organic Aerosol During Summertime in China, *J. Geophys. Res. Atmospheres*, 123, <https://doi.org/10.1029/2018JD029185>, 2018.

Schwantes, R. H., Emmons, L. K., Orlando, J. J., Barth, M. C., Tyndall, G. S., Hall, S. R., Ullmann, K., St. Clair, J. M., Blake, D. R., Wisthaler, A., and Bui, T. P. V.: Comprehensive isoprene and terpene gas-phase chemistry improves simulated surface ozone in the southeastern US, *Atmospheric Chem. Phys.*, 20, 3739–3776, <https://doi.org/10.5194/acp-20-3739-2020>, 2020.

630 Shilling, J. E., Zaveri, R. A., Fast, J. D., Kleinman, L., Alexander, M. L., Canagaratna, M. R., Fortner, E., Hubbe, J. M., Jayne, J. T., Sedlacek, A., Setyan, A., Springston, S., Worsnop, D. R., and Zhang, Q.: Enhanced SOA formation from mixed anthropogenic and biogenic emissions during the CARES campaign, *Atmospheric Chem. Phys.*, 13, 2091–2113, <https://doi.org/10.5194/acp-13-2091-2013>, 2013.

635 Shrivastava, M., Cappa, C. D., Fan, J., Goldstein, A. H., Guenther, A. B., Jimenez, J. L., Kuang, C., Laskin, A., Martin, S. T., Ng, N. L., Petaja, T., Pierce, J. R., Rasch, P. J., Roldin, P., Seinfeld, J. H., Shilling, J., Smith, J. N., Thornton, J. A., Volkamer, R., Wang, J., Worsnop, D. R., Zaveri, R. A., Zelenyuk, A., and Zhang, Q.: Recent advances in understanding secondary organic aerosol: Implications for global climate forcing, *Rev. Geophys.*, 55, 509–559, <https://doi.org/10.1002/2016RG000540>, 2017.

640 Shrivastava, M., Andreae, M. O., Artaxo, P., Barbosa, H. M. J., Berg, L. K., Brito, J., Ching, J., Easter, R. C., Fan, J., Fast, J. D., Feng, Z., Fuentes, J. D., Glasius, M., Goldstein, A. H., Alves, E. G., Gomes, H., Gu, D., Guenther, A., Jathar, S. H., Kim, S., Liu, Y., Lou, S., Martin, S. T., McNeill, V. F., Medeiros, A., De Sá, S. S., Shilling, J. E., Springston, S. R., Souza, R. A. F., Thornton, J. A., Isaacman-VanWertz, G., Yee, L. D., Ynoue, R., Zaveri, R. A., Zelenyuk, A., and Zhao, C.: Urban pollution greatly enhances formation of natural aerosols over the Amazon rainforest, *Nat. Commun.*, 10, 1046, <https://doi.org/10.1038/s41467-019-08909-4>, 2019.

645 Tilmes, S., Hodzic, A., Emmons, L. K., Mills, M. J., Gettelman, A., Kinnison, D. E., Park, M., Lamarque, J. -F., Vitt, F., Shrivastava, M., Campuzano-Jost, P., Jimenez, J. L., and Liu, X.: Climate Forcing and Trends of Organic Aerosols in the Community Earth System Model (CESM2), *J. Adv. Model. Earth Syst.*, 11, 4323–4351, <https://doi.org/10.1029/2019MS001827>, 2019.

Tong, D., Cheng, J., Liu, Y., Yu, S., Yan, L., Hong, C., Qin, Y., Zhao, H., Zheng, Y., Geng, G., Li, M., Liu, F., Zhang, Y., 650 Zheng, B., Clarke, L., and Zhang, Q.: Dynamic projection of anthropogenic emissions in China: methodology and 2015–2050 emission pathways under a range of socio-economic, climate policy, and pollution control scenarios, *Atmospheric Chem. Phys.*, 20, 5729–5757, <https://doi.org/10.5194/acp-20-5729-2020>, 2020.

Wang, L., Jin, X., Wang, Q., Mao, H., Liu, Q., Weng, G., and Wang, Y.: Spatial and temporal variability of open biomass burning in Northeast China from 2003 to 2017, *Atmospheric Ocean. Sci. Lett.*, 13, 240–247, 655 <https://doi.org/10.1080/16742834.2020.1742574>, 2020.

Xing, L., Fu, T.-M., Liu, T., Qin, Y., Zhou, L., Chan, C. K., Guo, H., Yao, D., and Duan, K.: Estimating organic aerosol emissions from cooking in winter over the Pearl River Delta region, China, *Environ. Pollut.*, 292, 118266, <https://doi.org/10.1016/j.envpol.2021.118266>, 2022.

Xu, B., Wang, T., Ma, D., Song, R., Zhang, M., Gao, L., Li, S., Zhuang, B., Li, M., and Xie, M.: Impacts of regional emission reduction and global climate change on air quality and temperature to attain carbon neutrality in China, *Atmospheric Res.*, 279, 660 106384, <https://doi.org/10.1016/j.atmosres.2022.106384>, 2022.

Xu, Z. N., Nie, W., Liu, Y. L., Sun, P., Huang, D. D., Yan, C., Krechmer, J., Ye, P. L., Xu, Z., Qi, X. M., Zhu, C. J., Li, Y. Y., Wang, T. Y., Wang, L., Huang, X., Tang, R. Z., Guo, S., Xiu, G. L., Fu, Q. Y., Worsnop, D., Chi, X. G., and Ding, A. J.: Multifunctional Products of Isoprene Oxidation in Polluted Atmosphere and Their Contribution to SOA, *Geophys. Res. Lett.*, 665 48, e2020GL089276, <https://doi.org/10.1029/2020GL089276>, 2021.

Yin, H., Pflugmacher, D., Li, A., Li, Z., and Hostert, P.: Land use and land cover change in Inner Mongolia - understanding the effects of China's re-vegetation programs, *Remote Sens. Environ.*, 204, 918–930, <https://doi.org/10.1016/j.rse.2017.08.030>, 2018.

Yue, M., Dong, X., Wang, M., Emmons, L. K., Liang, Y., Tong, D., Liu, Y., and Liu, Y.: Modeling the Air Pollution and 670 Aerosol-PBL Interactions Over China Using a Variable-Resolution Global Model, *J. Geophys. Res. Atmospheres*, 128, e2023JD039130, <https://doi.org/10.1029/2023JD039130>, 2023.

Zaveri, R. A., Easter, R. C., Fast, J. D., and Peters, L. K.: Model for Simulating Aerosol Interactions and Chemistry (MOSAIC), *J. Geophys. Res. Atmospheres*, 113, 2007JD008782, <https://doi.org/10.1029/2007JD008782>, 2008.

Zaveri, R. A., Easter, R. C., Singh, B., Wang, H., Lu, Z., Tilmes, S., Emmons, L. K., Vitt, F., Zhang, R., Liu, X., Ghan, S. J., 675 and Rasch, P. J.: Development and Evaluation of Chemistry-Aerosol-Climate Model CAM5-Chem-MAM7-MOSAIC: Global Atmospheric Distribution and Radiative Effects of Nitrate Aerosol, *J. Adv. Model. Earth Syst.*, 13, e2020MS002346, <https://doi.org/10.1029/2020MS002346>, 2021.

Zhang, G. J. and McFarlane, N. A.: Sensitivity of climate simulations to the parameterization of cumulus convection in the Canadian climate centre general circulation model, *Atmosphere-Ocean*, 33, 407–446, 680 <https://doi.org/10.1080/07055900.1995.9649539>, 1995.

Zhang, H., Yee, L. D., Lee, B. H., Curtis, M. P., Worton, D. R., Isaacman-VanWertz, G., Offenberg, J. H., Lewandowski, M., Kleindienst, T. E., Beaver, M. R., Holder, A. L., Lonneman, W. A., Docherty, K. S., Jaoui, M., Pye, H. O. T., Hu, W., Day, D. A., Campuzano-Jost, P., Jimenez, J. L., Guo, H., Weber, R. J., De Gouw, J., Koss, A. R., Edgerton, E. S., Brune, W., Mohr, C., Lopez-Hilfiker, F. D., Lutz, A., Kreisberg, N. M., Spielman, S. R., Hering, S. V., Wilson, K. R., Thornton, J. A., and 685 Goldstein, A. H.: Monoterpenes are the largest source of summertime organic aerosol in the southeastern United States, *Proc. Natl. Acad. Sci.*, 115, 2038–2043, <https://doi.org/10.1073/pnas.1717513115>, 2018.

Zhang, J.: New formation and fate of Isoprene SOA markers revealed by field data-constrained modeling, 2023.

Zhang, Q., Jimenez, J. L., Canagaratna, M. R., Allan, J. D., Coe, H., Ulbrich, I., Alfarra, M. R., Takami, A., Middlebrook, A. M., Sun, Y. L., Dzepina, K., Dunlea, E., Docherty, K., DeCarlo, P. F., Salcedo, D., Onasch, T., Jayne, J. T., Miyoshi, T.,
690 Shimono, A., Hatakeyama, S., Takegawa, N., Kondo, Y., Schneider, J., Drewnick, F., Borrmann, S., Weimer, S., Demerjian, K., Williams, P., Bower, K., Bahreini, R., Cottrell, L., Griffin, R. J., Rautiainen, J., Sun, J. Y., Zhang, Y. M., and Worsnop, D. R.: Ubiquity and dominance of oxygenated species in organic aerosols in anthropogenically-influenced Northern Hemisphere midlatitudes, *Geophys. Res. Lett.*, 34, 2007GL029979, <https://doi.org/10.1029/2007GL029979>, 2007.

Zheng, B., Tong, D., Li, M., Liu, F., Hong, C., Geng, G., Li, H., Li, X., Peng, L., Qi, J., Yan, L., Zhang, Y., Zhao, H., Zheng, Y., He, K., and Zhang, Q.: Trends in China's anthropogenic emissions since 2010 as the consequence of clean air actions, *Atmospheric Chem. Phys.*, 18, 14095–14111, <https://doi.org/10.5194/acp-18-14095-2018>, 2018.

Zheng, H., Chang, X., Wang, S., Li, S., Zhao, B., Dong, Z., Ding, D., Jiang, Y., Huang, G., Huang, C., An, J., Zhou, M., Qiao, L., and Xing, J.: Sources of Organic Aerosol in China from 2005 to 2019: A Modeling Analysis, *Environ. Sci. Technol.*, 57, 5957–5966, <https://doi.org/10.1021/acs.est.2c08315>, 2023a.

700 Zheng, H., Chang, X., Wang, S., Li, S., Yin, D., Zhao, B., Huang, G., Huang, L., Jiang, Y., Dong, Z., He, Y., Huang, C., and Xing, J.: Trends of Full-Volatility Organic Emissions in China from 2005 to 2019 and Their Organic Aerosol Formation Potentials, *Environ. Sci. Technol. Lett.*, 10, 137–144, <https://doi.org/10.1021/acs.estlett.2c00944>, 2023b.

Zhong, Y., Chen, J., Zhao, Q., Zhang, N., Feng, J., and Fu, Q.: Temporal trends of the concentration and sources of secondary organic aerosols in PM2.5 in Shanghai during 2012 and 2018, *Atmos. Environ.*, 261, 118596,
705 <https://doi.org/10.1016/j.atmosenv.2021.118596>, 2021.

Zhuang, Y., Li, R., Yang, H., Chen, D., Chen, Z., Gao, B., and He, B.: Understanding Temporal and Spatial Distribution of Crop Residue Burning in China from 2003 to 2017 Using MODIS Data, *Remote Sens.*, 10, 390, <https://doi.org/10.3390/rs10030390>, 2018.